Mutations in the EF-Hand Motif Impair the Inactivation of Barium Currents of the Cardiac α_{1C} Channel

G. Bernatchez, D. Talwar, and L. Parent
Département de Physiologie, Membrane Transport Research Group, Université de Montréal, Montréal, Québec H3C 3J7, Canada

ABSTRACT Calcium-dependent inactivation has been described as a negative feedback mechanism for regulating voltage-dependent calcium influx in cardiac cells. Most recent evidence points to the C-terminus of the α_{1C} subunit, with its EF-hand binding motif, as being critical in this process. The EF-hand binding motif is mostly conserved between the C-termini of six of the seven α_1 subunit Ca^{2+} channel genes. The role of E1537 in the C-terminus of the α_{1C} calcium channel inactivation was investigated here after expression in *Xenopus laevis* oocytes. Whole-cell currents were measured in the presence of 10 mM Ba^{2+} or 10 mM Ca^{2+} after intracellular injection of 1,2-bis(2-aminophenoxy)ethane-*N,N,N′,N′*-tetraacetic acid. Against all expectations, our results showed a significant reduction in the rate of voltage-dependent inactivation as measured in Ba^{2+} solutions for all E1537 mutants, whereas calcium-dependent inactivation appeared unscathed. Replacing the negatively charged glutamate residue by neutral glutamine, glycine, serine, or alanine significantly reduced the rate of Ba^{2+}-dependent inactivation by 1.5-fold (glutamine) to 3.5-fold (alanine). The overall rate of macroscopic inactivation measured in Ca^{2+} solutions was also reduced, although a careful examination of the distribution of the fast and slow time constants suggests that only the slow time constant was significantly reduced in the mutant channels. The fast time constant, the hallmark of Ca^{2+}-dependent inactivation, remained remarkably constant among wild-type and mutant channels. Moreover, inactivation of E1537A channels, in both Ca^{2+} and Ba^{2+} solutions, appeared to decrease with membrane depolarization, whereas inactivation of wild-type channels became faster with positive voltages. All together, our results showed that E1537 mutations impaired voltage-dependent inactivation and suggest that the proximal part of the C-terminus may play a role in voltage-dependent inactivation in L-type α_{1C} channels.

INTRODUCTION

Calcium ion influx through the voltage-dependent calcium channel plays a major role in the excitation-contraction coupling of cardiac myocytes. To date, molecular cloning has identified the primary structures for seven to nine distinct calcium channel α_1 subunits (α_{1A}, α_{1B}, α_{1C}, α_{1D}, α_{1E}, α_{1F}, α_{1G}, α_{1H}, α_{1S}) (Hofmann et al., 1994; Perez-Reyes et al., 1998; Tsien, 1998). The α_1 subunit of the cardiac L-type calcium channel has been cloned (Perez-Reyes, 1990; Wei et al., 1991). Reminiscent of the native channel, the α_{1C} subunit, whether expressed in *Xenopus* oocytes or in mammalian HEK-293 cells, typically inactivates faster in the presence of Ca^{2+} than in the presence of Ba^{2+} ions (Neely et al., 1994; Parent et al., 1995; DeLeon et al., 1995). In contrast, α_{1E} channels showed similar rates of inactivation in the presence of Ba^{2+} and Ca^{2+} (Parent et al., 1997). Several mechanisms have been proposed to explain Ca^{2+}-dependent inactivation. Single-channel data strongly suggest that calcium-dependent inactivation is triggered by Ca^{2+} ions binding directly to the intracellular face of the channel (Imredy and Yue, 1994). Inactivation is rapid and calcium sensitive in patches with a single L-type calcium channel (Imredy and Yue, 1992) and in planar lipid bilayers (Haack and Rosenberg, 1994). Calcium influx through one L-type calcium channel can therefore selectively facilitate the inactivation of another adjacent channel without a generalized elevation of bulk intracellular calcium concentration (Imredy and Yue, 1992; Risso and DeFelice, 1993). For instance, in cardiac cells, local internal Ca^{2+} is elevated from baseline values of 0.05 μM to peak values of 7 μM after opening of voltage-dependent calcium channels (Risso and DeFelice, 1993; Cannell et al., 1995; Lòpez-Lòpez et al., 1995). A sharp decrease in the free intracellular concentration of Ca^{2+} could also slow and/or reduce calcium-dependent inactivation, prompting the suggestion that Ca^{2+} acts from the internal face of the channel (Kramer et al., 1991). Furthermore, intracellular perfusion with trypsin was shown to decrease Ca^{2+}-dependent inactivation in guinea pig myocytes (You et al., 1995), suggesting the presence of a intracellular "Ca^{2+}-dependent inactivation particle" similar to the "ball-and-chain" inactivation particle of *Shaker* K^+ channels (Hoshi et al., 1990). Thus Ca^{2+} binding could occur at a site with a high affinity (Johnson and Byerly, 1993) or a site with moderate affinity close enough to the calcium channel pore, such as the channel inner mouth. Direct binding of Ca^{2+} to the channel protein would thus be consistent with most experimental results and has emerged as the most likely chemical initiation event for inactivation.

It has therefore been suggested that calcium binding sites in cytoplasmic domains are critical in calcium-dependent inactivation, with a possible role for the C-terminus of α_{1C}. Ca^{2+} ions can interact with neutral oxygen donors such as

Received for publication 29 August 1997 and in final form 7 July 1998.

Address reprint requests to Dr. Lucie Parent, Département de Physiologie, Membrane Transport Research Group, Université de Montréal, P.O. Box 6128, Downtown Station, Montréal, Québec H3C 3J7, Canada. Tel.: 514-343-6111, ext. 4354; Fax: 514-343-7146; E-mail: parentlu@alize.ere.umontreal.ca.

0006-3495/98/10/1727/13 $2.00

carbonyl and alcohol groups with a coordination number varying between 6 and 8 (DaSilva and Williams, 1993). The major ligands in calcium-binding proteins are thus oxygen-containing residues with either carboxylate groups (aspartate, glutamate) or carboxyl groups (asparagine, glutamine, serine, threonine), as in calmodulin and parvalbumin (McPhalen et al., 1991; Nakayama et al., 1992). The calcium binding motif recurrent in these proteins is called an EF-hand binding motif. Functional EF-hands occur in pairs, with the two hands (α-helices) related by an approximate twofold axis of symmetry around a calcium-loop binding site. EF-hand proteins bind Ca^{2+} with dissociation constants in the micromolar (μM) range (Kretsinger, 1976; Kohama, 1979), which is compatible with the reported observation that intracellular Ca^{2+} causes inactivation with a $K_d \approx 4$ μM (Haack and Rosenberg, 1994). The C-terminus of all calcium channel α_1 subunits has retained the sequence of a EF-hand motif in a section located close to IVS6 (Babitch, 1990). It shows high sequence similarity to Ca^{2+} binding sites in its central region, where Ca^{2+} binding is contributed by a hydrophilic residue (aspartate, asparagine, glutamate, glutamine, serine, threonine). The proposition that a EF-hand binding motif in the C-terminus may play a active role in calcium-dependent inactivation is thus quite attractive, as it meets the basic criteria of intracellular calcium binding site requirements. Indeed, a role for the EF-hand binding motif in calcium-dependent inactivation was first suggested by chimeric studies conducted by DeLeon and colleagues (1995). Amino acid sequences in the C-terminus are shown in Fig. 1 for $\alpha_{1C,}$ α_{1D}, α_{1A}, α_{1B}, and α_{1E} calcium channel subunits. The C-terminus of α_{1G} is not shown, as it does not bear any homology to the other α_1 subunits (Perez-Reyes et al., 1998). The inferred calcium ligands are assigned to the vertices of an octahedron as *X*, *Y*, *Z*, $-Y$, $-X$, $-Z$ and are provided by oxygen-containing side chains. Residues that comply with the consensus sequence are underlined. As seen, residues K1539 and K1543 in α_{1C} fail to comply with the classical model of an EF-hand motif. However, the ligand found at the *Y* position, which corresponds to amino acid E1537 in α_{1C}, is replaced by a hydrophobic alanine residue in α_{1A}, α_{1B}, and α_{1E} channels that all lack faster calcium-dependent inactivation (DeWaard and Campbell, 1995; Parent et al., 1997). Herein the role of the glutamate residue E1537 was tested with a series of point mutations to document the nature of Ca^{2+} binding, if any, at this site. Inactivation data reported herein most unexpectedly suggest that the residues within the EF-hand binding motif may rather contribute to voltage-dependent inactivation in α_{1C} channels.

MATERIALS AND METHODS

Polymerase chain reaction mutagenesis for E1537 mutants

Standard methods of plasmid DNA preparation and DNA sequencing were used (Sambrook et al., 1989). A wild-type, full-length cardiac α_{1C} subunit cDNA (Genebank X15539) was cloned from rabbit (Wei et al., 1991). Point mutations were prepared by overlap extension at the junctions of the relevant domains, using sequential polymerase chain reaction (PCR) (Hoffman–La Roche) (Ho et al., 1989) as described earlier (Parent et al., 1995; Parent and Gopalakrishnan, 1995). Briefly, 1.1-kbp DNA fragments were amplified between nucleotides 3752 and 5236 from the full-length α_{1C} template, using Gold Ampli-Taq polymerase (Perkin-Elmer Cetus) in reactions performed with a DNA Thermal Cycler 2400 (Perkin-Elmer Cetus) or a DNA engine PTC-200 (MJ Research). The final PCR product containing the overlapping region was ligated back into the host α_{1C} subunit between the *Eco*RV (4350) and *Bst*EII (4646) sites. Restriction enzymes were obtained from New England Biolabs (Beverly, MA). Constructs were verified by restriction mapping, and recombinant clones were screened by double-stranded sequence analysis of the entire ligated cassette. DNA constructs were linearized at the 3′ end by *Hin*dIII digestion, and run-off transcripts were prepared using methylated cap analog $m^7G(5')ppp(5')G$ and T7 RNA polymerase included in the mMessage mMachine transcription kit (Ambion, Austin, TX). The final cRNA products were resuspended in 0.1 M KCl at a concentration of 2 $\mu g/\mu l$ and stored at -80°C. The integrity of the final product and the absence of degraded RNA were determined by denaturing agarose gel stained with ethidium bromide.

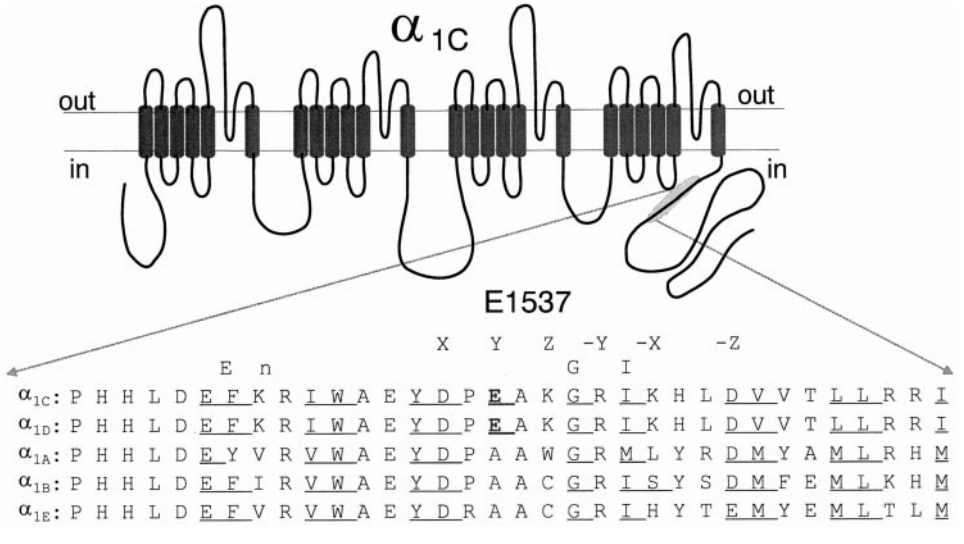

FIGURE 1 Predicted secondary structure for the cardiac α_{1C} channel with the four homologous repeats I, II, III, IV. The N- and C-termini are predicted to be facing the cytoplasm. The E1537 residue is located within 100 nucleotides (or 30 AA) of the IVS6 transmembrane segment in a short section of the C-terminus that bears high homology to a Ca^{2+}-binding motif. The amino acid alignment for α_{1C}, α_{1D}, α_{1A}, α_{1B}, and α_{1E} calcium channels is shown enlarged for this section of the C-terminus. The EF-hand binding motif is absent in the newly cloned α_{1G} channel. There is a high degree of homology between the calcium channel α_1 subunits, with a few notable exceptions, such as E1537.

Functional expression of wild-type and E1537 mutant channels

Oocytes were obtained from female *Xenopus laevis* clawed frog (Nasco, Fort Atkinson, WI) as described previously (Parent et al., 1995, 1997; Parent and Gopalakrishnan, 1995). Individual oocytes free of follicular cells were obtained after 30–40 min of incubation in a calcium-free saline solution (in mM: 82.5 NaCl; 2.5 KCl; 1 $MgCl_2$; 5 HEPES; pH 7.6) containing 2 mg/ml collagenase (Sigma-Aldrich, St. Louis, MO). Forty-seven nanoliters of cRNA coding for the wild-type or mutated α_{1C} subunit was injected 16 h later at a concentration of 100 ng/μl in 0.1 M KCl (4.7 ng total cRNA) into stage V and VI oocytes. cRNA coding for rat brain $\alpha_{2b}\delta$ (Williams et al., 1992) and rat brain/cardiac β_{2a} (Perez-Reyes et al., 1992) was typically coinjected with α_{1C} at a 1:1:1 molar ratio. Oocytes were incubated at 18°C in a Barth solution (in mM): 88 NaCl; 3 KCl; 0.82 $MgCl_2$; 0.41 $CaCl_2$; 0.33 $Ca(NO_3)_2$; 5 HEPES; pH 7.6, supplemented with 5% horse serum, 2.5 mM Na pyruvate, 100 units/ml penicillin; 0.1 mg/ml streptomycin.

Electrophysiological recordings and result analysis

Wild-type and mutant α_{1C} channels were screened for macroscopic barium current 4–7 days after RNA injection, with the Warner OC-725C amplifier oocyte clamp as desribed earlier (Parent et al., 1995, 1997). Voltage and current electrodes, filled with 3 M KCl, were broken slightly under the microscope to decrease the electrode resistance to 1.5 MΩ tip resistance. Whole-cell currents were measured at room temperature in a 10 BaMeS solution (in mM: 10 $Ba(OH)_2$; 110 NaOH; 1 KOH; 0.5 niflumic acid; 10 HEPES titrated to pH 7.2 with methanesulfonic acid) or a 10 CaMeS solution in which $Ca(OH)_2$ replaced $Ba(OH)_2$ equimolarly. Niflumic acid was added to block endogenous Ca^{2+}-dependent Cl^- currents (White and Aylwin, 1990). To further palliate contamination by these Cl^- currents, a volume of 100 nl of a 10 mM 1,2-bis(2-aminophenoxy)ethane-*N*,*N*,*N*′,*N*′-tetraacetic acid titrated with HEPES and KOH to pH 7.4 (BAPTA-HEPES) stock solution was injected directly into oocytes 1–2 h before experiments for a final concentration of 1 mM. Alternatively, oocytes were also preincubated in a saline solution containing 100 μM 1,2-bis(2-aminophenoxy)ethane-*N*,*N*,*N*′,*N*′-tetraacetic acid tetra lacetoxymethyl) ester (BAPTA-AM) (Sigma-Aldrich, St. Louis, MO). Whole-cell current traces were filtered at 1 kHz, using the built-in filter of the oocyte clamp, and were acquired at 5 kHz through a Digidata 1200 analogue-to-digital board (Axon Instruments, CA). The pClamp programs Clampex and Clampfit, version 6.04, were used to generate voltage protocols and to digitally acquire and analyze data. Capacitive transients and leak currents were digitally subtracted. Isochronic inactivation curves were generated by measuring tail currents obtained after 5-s voltage pulses applied from −100 to +30 mV. Fractional currents were fitted to Eq. 1 (Parent et al., 1995, 1997):

$$\frac{i}{i_{max}} = 1 - \frac{1 - Y_o}{1 + \left\{\exp\frac{-zF(V_m - E_{0.5})}{RT}\right\}} \qquad (1)$$

where i is the peak current obtained after a 5-s pulse to voltage V_m; i_{max} is the peak current measured after a 5-s voltage pulse to −100 mV; and i/i_{max} is their ratio when normalized to 1; Y_0 is the fraction of noninactivating current; $E_{0.5}$ is the midpotential of inactivation; z is the slope factor; and R, T, F have their usual meanings. Pooled data points i/i_{max} (mean ± SEM) were fitted to this modified Boltzmann equation using user-defined functions and the fitting algorithms provided in Origin 5.0 (Microcal Software) analysis software. Fit parameters were estimated with their corresponding errors. For the activation and inactivation time constants, leak subtracted current traces recorded at 10 kHz were fitted with exponential functions of the first order for Ba^{2+} currents (Eq. 2) or the second order for Ca^{2+} currents (Eq. 3), using the Chebyshev algorithm in Clampfit 6.04. Whole-cell Ba^{2+} current time constants were systematically measured between time $t = 0$ s and $t = 2$ s with the following equation:

$$I(t) = I_{act}\exp\left(-\frac{t}{\tau_{act}}\right) + I_{inact}\exp\left(-\frac{t}{\tau_{inact}}\right) + C \qquad (2)$$

I(t) is the current at time t; τ_{act} and τ_{inact} are the time constants of the activation and inactivation processes, and I_{act} and I_{inact} are the amplitudes of these processes. For simplicity's sake, the single inactivation time constant measured in Ba^{2+} is often referred to as τ^{inact}_{Ba} in the text. Whole-cell Ca^{2+} current time constants were measured between time $t = 0$ and $t = 2$ s with the following equation:

$$I(t) = I_{act}\exp\left(-\frac{t}{t_{act}}\right) + I^1_{inact}\exp\left(-\frac{t}{\tau^1_{inact}}\right) + I^2_{inact}\exp\left(-\frac{t}{\tau^2_{inact}}\right) + C \qquad (3)$$

$I(t)$ is the current at time t; τ_{act}, τ^1_{inact}, and τ^2_{inact} are the time constants of the activation, the fast inactivation, and the slow inactivation processes, respectively; I_{act}, I^1_{inact}, and I^2_{inact} are the amplitudes of the same processes. For simplicity's sake, the two inactivation time constants measured in Ca^{2+} are referred to, respectively, as τ^{inact}_{fast} and τ^{inact}_{slow} in the text. Experiments were performed at room temperature. Figures were drawn using Designer 4.1 (Micrografx Software).

RESULTS

Fig. 1 compares the primary sequences of the C-termini of α_{1C}, α_{1D}, α_{1A}, α_{1B}, and α_{1E} subunits. The C-terminus of the newly cloned T-type calcium channel α_{1G} (Perez-Reyes et al., 1998) does not exhibit a putative EF-hand binding motif. The rationale for targeting the putative EF-hand motif in calcium-dependent inactivation pertains to its potential ability to form an intracellular Ca^{2+} binding site. In particular, we were interested in the E ⇒ A mutation at position 1537. Alanine is a small, neutral, relatively hydrophobic residue, whereas glutamate is a hydrophilic (acidic) residue with a pK_a value of 4.3 that would thus be negatively charged under physiological conditions. Acidic residues are also known to be effective chelators of metal ions such as Ca^{2+} and Cd^{2+} (Creighton, 1993). Thus the respective side chains of alanine and glutamate are expected to display large differences in their Ca^{2+} affinity, regardless of their role in the putative EF-hand. If position 1537 were critical in calcium-dependent inactivation, substitution at this position by a less polar residue could significantly slow Ca^{2+}-dependent inactivation while leaving Ba^{2+}-dependent inactivation unaltered.

E1537 mutant channels displayed slower inactivation kinetics in Ba^{2+} and Ca^{2+} solutions

To investigate the possible role of the negatively charged E1537 residue in calcium-dependent inactivation, mutant channels E1537D, E1537Q, E1537S, E1537G, and E1537A were expressed in *Xenopus* oocytes. Fig. 2 shows typical whole-cell current recordings, for the wild-type and mutant E1537Q, E1537S, E1537A cardiac α_{1C} calcium channels,

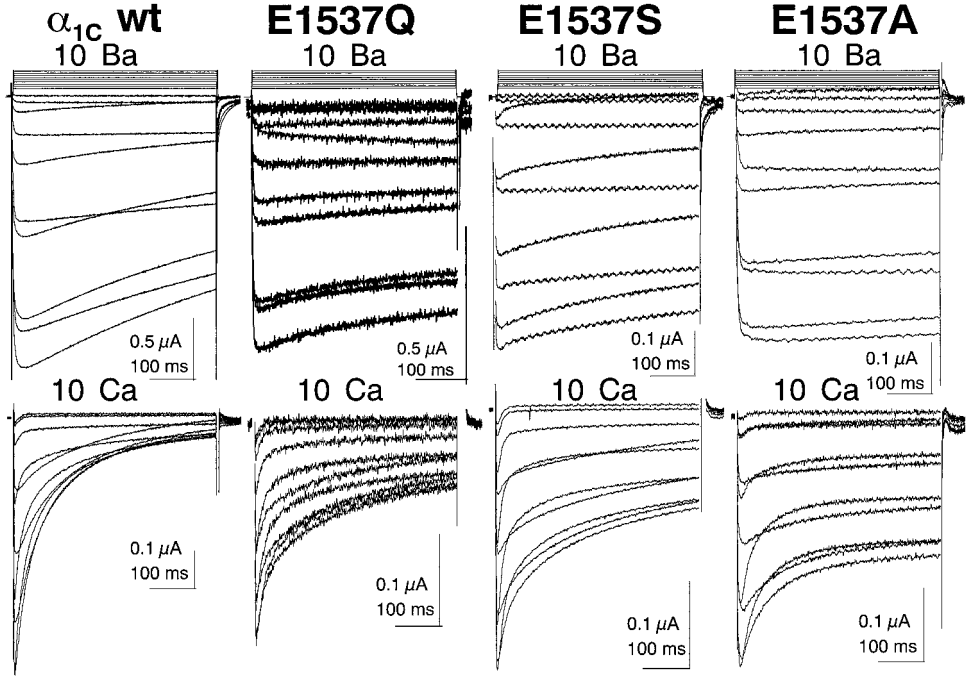

FIGURE 2 The whole-cell current α_{1C} kinetics are faster in the presence of Ca^{2+} as the charge carrier. Wild-type α_{1C} and mutant E1537Q, E1537S, E1537A were expressed in *Xenopus* oocytes with auxiliary $\alpha_{2b}\delta$ and β_{2a} subunits. The current traces were recorded with the two-electrode voltage-clamp technique, 2 h after injection of 10 mM BAPTA, in the presence of 10 mM Ba^{2+} (*top traces*) and 10 mM Ca^{2+} (*bottom traces*). The holding potential was −80 mV throughout. Voltage pulses (450 ms) were applied from −40 to +50 mV in 10-mV steps at 0.2 Hz. In all channels, wild-type and mutants, calcium traces were always faster than barium traces. Leak currents were digitally subtracted. Capacitive transients were erased for the first millisecond after the voltage step. The current scale varies between 0.05 and 0.5 μA. Time scales are 100 ms throughout.

obtained in the presence of 10 mM Ba^{2+} (*top*) or 10 mM Ca^{2+} (*bottom*) solutions, using 450 ms voltage steps. In these and the following experiments, the α_{1C} subunits (wild-type and mutants) were systematically coinjected with the $\alpha_{2b}\delta$ and the β_{2a} auxiliary subunits. Except for the E1537D mutant, for which we never got expression, all E1537 mutant yielded measurable Ba^{2+} and Ca^{2+} currents with bona fide Ca^{2+} channel characteristics (see also later in Fig. 4). Peak Ba^{2+} currents ranged from 400 to 900 nA (see Table 1). Although such current amplitudes are well above background, E1537 mutant peak current amplitude was on average twofold smaller than the wild-type α_{1C} peak current recorded under the same experimental conditions. In addition, macroscopic Ba^{2+} currents were at least twice as large as Ca^{2+} currents in all mutants. This ratio likely represents a minimum value, as Ca^{2+} currents were generally recorded a few days later than Ba^{2+} currents to improve the signal-to-noise ratio. Macroscopic Ba^{2+} currents activated within 3 ms. As expected for L-type cardiac calcium channels, the macroscopic wild-type α_{1C} currents typically inactivated faster in the presence of 10 mM Ca^{2+} than in the presence of Ba^{2+} (*left*). In fact, all channels displayed a faster Ca^{2+}-dependent than Ba^{2+}-dependent inactivation, as Ba^{2+} currents invariably inactivated more slowly than the corresponding Ca^{2+} traces, from the wild-type to the E1537A channel. This observation also applied to E1537G whole-cell currents that are not shown in this figure. Six independent series of channel expression in oocytes confirmed these observations. The slower Ba^{2+}- and Ca^{2+}-dependent inactivation in E1537A channels was also observed in the presence of the β_3 subunit (Castellano et al., 1993) (results not shown), indicating that the reduced inactivation was independent of the nature of the β subunit. Based on the observation that inactivation remained faster in the presence of Ca^{2+}, one may reasonably conclude that calcium-dependent inactivation was not abolished by mutations at position E1537, a conclusion also reached by Zhou and colleagues (1997). A careful examination of the whole-cell recordings nonetheless indicates that both Ba^{2+} and Ca^{2+} current traces inactivated faster for the wild-type than for the mutant channels in the following order: wt > E1537Q > E1537S ≫ E1537A, thus suggesting that overall macroscopic inactivation was reduced for E1537 mutant channels. Indeed, all mutant channels displayed significantly slower kinetics than the wild-type α_{1C} calcium channel. To investigate and quantify the mutant channel kinetics, whole-cell Ba^{2+} and Ca^{2+} currents were fitted to a sum of exponential functions (see Table 2 and Fig. 3). Inactivation time con-

TABLE 1 Whole-cell peak currents for wild-type $\alpha_{1C}/\alpha_{2b}\delta/\beta_{2a}$, E1537A/$\alpha_{2b}\delta/\beta_{2a}$, E1537G/$\alpha_{2b}\delta/\beta_{2a}$, E1537Q/$\alpha_{2b}\delta/\beta_{2a}$, and E1537S/$\alpha_{2b}\delta/\beta_{2a}$ channels in 10 mM Ba^{2+} and 10 mM Ca^{2+} solutions as the mean ± SEM of *n* independent experiments

	Wild-Type	E1537A	E1537G	E1537Q	E1537S
10 Ba	1.3 ± 0.2 (11)	0.87 ± 0.06 (15)	0.38 ± 0.06 (7)	0.63 ± 0.04 (24)	0.44 ± 0.04 (8)
10 Ca	0.61 ± 0.08 (14)	0.43 ± 0.05 (14)	0.25 ± 0.03 (5)	0.27 ± 0.04 (11)	0.28 ± 0.03 (7)

Whole-cell currents were typically larger for the wild-type channel. Moreover, Ba^{2+} currents were at least twice as large as Ca^{2+} currents. The 2:1 Ba^{2+}-to-Ca^{2+} ratio was a minimum, because Ca^{2+} experiments were usually performed 2–3 days later than Ba^{2+} experiments to work with the largest possible Ca^{2+} currents.

TABLE 2 Inactivation time constants for wild-type $\alpha_{1C}/\alpha_{2b}\delta/\beta_{2a}$, E1537Q/$\alpha_{2b}\delta/\beta_{2a}$, E1537G/$\alpha_{2b}\delta/\beta_{2a}$, E1537S/$\alpha_{2b}\delta/\beta_{2a}$, and E1537A/$\alpha_{2b}\delta/\beta_{2a}$ channels recorded in 10 mM Ba^{2+} or 10 mM Ca^{2+} solutions

Channels	τ_{Ba}^{inact} (ms)	τ_{fast}^{inact} Ca^{2+} (ms)	A_{fast} Ca^{2+}	τ_{slow}^{inact} Ca^{2+} (ms)	A_{slow} Ca^{2+}
wt $\alpha_{1C}/\alpha_{2b}\delta/\beta_{2a}$	672 ± 43 (7)	49 ± 2 (15)	59 ± 4%	496 ± 33 (15)	41 ± 4%
E1537Q/$\alpha_{2b}\delta/\beta_{2a}$	780 ± 26 (6)*	64 ± 10 (6)*	45 ± 6%	640 ± 9 (6)***	55 ± 6%
E1537G/$\alpha_{2b}\delta/\beta_{2a}$	876 ± 40 (5)**	69 ± 11 (5)*	40 ± 3%	701 ± 18 (5)***	60 ± 3%
E1537S/$\alpha_{2b}\delta/\beta_{2a}$	988 ± 40 (5)**	55 ± 9 (6)*	37 ± 5%	712 ± 41 (6)***	63 ± 5%
E1537A/$\alpha_{2b}\delta/\beta_{2a}$	2501 ± 740 (5)**	56 ± 3 (12)*	35 ± 7%	2372 ± 659 (12)***	65 ± 7%

Whole-cell current traces recorded at $V_m = +10$ mV were fitted to single-exponential (Ba^{2+}) or double-exponential (Ca^{2+}) functions at time $t = 2$ s (see Eq. 3). Time constants are shown as the mean ± SEM, with the number n of independent measures. The relative amplitude of each exponential function used to describe the Ca^{2+} inactivation time course is shown as A_{slow} (I^2_{inact}) and A_{fast} (I^1_{inact}). The fast Ca^{2+} inactivation time constants (τ_{fast}) are not significant at the level $p < 0.1$ (*).

stants at $V_m = +10$ mV were estimated at time $t = 2$ s for wild-type $\alpha_{1C}/\alpha_{2b}\delta/\beta_{2a}$; E1537Q/$\alpha_{2b}\delta/\beta_{2a}$, E1537G/$\alpha_{2b}\delta/\beta_{2a}$, E1537S/$\alpha_{2b}\delta/\beta_{2a}$, and E1537A/$\alpha_{2b}\delta/\beta_{2a}$ channels in the presence of 10 mM Ba^{2+} (*right panel*) or 10 mM Ca^{2+} (*left panel*). As shown in the right panel of Fig. 3, the inactivation time course of whole-cell Ba^{2+} traces could be fit well by a single exponential function. Ba^{2+} inactivation time constants increased from 672 ± 43 ms ($n = 7$) for the wild-type α_{1C} channel to 988 ± 40 ms ($n = 5$) for E1537S and to 2501 ± 740 ms ($n = 5$) for E1537A. As seen, all E1537 mutant channels displayed significantly slower Ba^{2+} inactivation than the wild-type channel. Indeed, τ_{Ba}^{inact} for the wild-type channel was different from the E1537Q channel time constant at the level $p < 0.1$ (*), whereas they were significantly different at the level $p < 0.05$ (**) for E1537G, E1537S, and E1537A channels. The inactivation time course of whole-cell Ca^{2+} traces required, in contrast, at least a sum of two exponential functions τ_{fast}^{inact} and τ_{slow}^{inact}. The faster inactivation time constant τ_{fast}^{inact} was not significantly affected by mutations at E1537 as τ_{fast}^{inact} ranged from 49 ± 2 ms ($n = 15$) for the wild-type channel to 56 ± 3 ms ($n = 12$) for E1537A. On the other hand, the slower Ca^{2+} inactivation time constant τ_{slow}^{inact} increased from 496 ± 33 ms ($n = 15$) for the wild-type α_{1C} channel to 712 ± 41 ms ($n = 6$) for E1537S and to 2378 ± 660 ms ($n = 12$) for E1537A. The increase in τ_{slow}^{inact} in the E1537A mutant was accompanied by a parallel increase in its relative importance as the relative amplitude of the slower Ca^{2+} inactivation time constant increased from 41 ± 4% for the wild-type channel to 65 ± 7% for E1537A. The fit values, including the relative amplitudes of τ_{fast}^{inact} and τ_{slow}^{inact}, are given in detail in Table 2. From our whole-cell recordings, it thus appears that

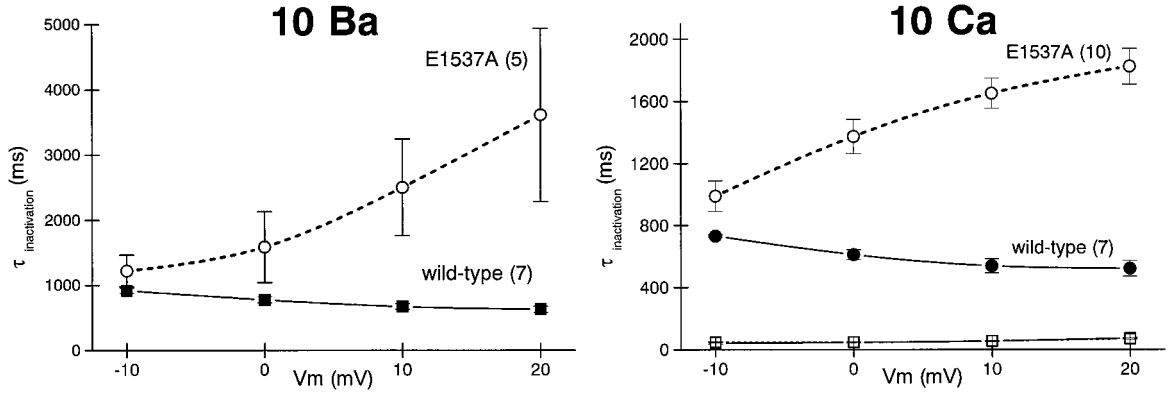

FIGURE 3 Mutations at E1537 slowed α_{1C} inactivation in Ba^{2+} and Ca^{2+}. In the presence of Ba^{2+}, two exponential functions can satisfactorily account for the current time course, whereas the current time course in the presence of Ca^{2+} could be best described by a sum of three exponential functions (τ_{act}, τ_{fast}^{inact}, τ_{slow}^{inact}) for all channels herein investigated. Only the inactivation time constants are reported here. Inactivation time constants for $V_m = +10$ mV were estimated at time $t = 2$ s for wild-type $\alpha_{1C}/\alpha_{2b}\delta/\beta_{2a}$; E1537Q/$\alpha_{2b}\delta/\beta_{2a}$, E1537G/$\alpha_{2b}\delta/\beta_{2a}$, E1537S/$\alpha_{2b}\delta/\beta_{2a}$, and E1537A/$\alpha_{2b}\delta/\beta_{2a}$ channels in the presence of 10 mM Ba^{2+} (*right*) or 10 mM Ca^{2+} (*left*). (*Right*) Inactivation time course of whole-cell Ba^{2+} traces could be well fitted by a single exponential time constant. Ba^{2+} inactivation time constants increased from 672 ± 43 ms ($n = 7$) for the wild-type α_{1C} channel to 988 ± 40 ms ($n = 5$) for E1537S and to 2501 ± 740 ms ($n = 5$) for E1537A. All mutant channel inactivated significantly more slowly in Ba^{2+} than did the wild-type channel. The fit values are given in detail in Table 2. (*Left*) Inactivation time course of whole-cell Ca^{2+} traces could be best described by a sum of two exponential functions. The faster inactivation time constant τ_{fast}^{inact} was not significantly affected by mutations at E1537 as τ_{fast}^{inact} ranged from 49 ± 2 ms ($n = 15$) for the wild-type channel to 56 ± 3 ms ($n = 12$) for E1537A. On the other hand, the slower Ca^{2+} inactivation time constant τ_{slow}^{inact} increased from 496 ± 33 ms ($n = 15$) for the wild-type α_{1C} channel to 712 ± 41 ms ($n = 6$) for E1537S and to 2378 ± 660 ms ($n = 12$) for E1537A. Moreover, the relative amplitude of the slower Ca^{2+} inactivation time constant increased from 41 ± 4% for the wild-type channel to 65 ± 7% for E1537A. τ_{slow}^{inact} was different from the wild-type channel at the significance level $p < 0.01$ (***) for all E1537 mutant channels, whereas τ_{fast}^{inact} was not significantly different at the level $p < 0.1$. τ_{Ba}^{inact} for E1537Q was different at the level $p < 0.1$ (*), and τ_{Ba}^{inact} for E1537G, E1537S, and E1537A was different at the level $p < 0.05$ (**). The fit values, including the relative amplitude of τ_{fast}^{inact} and τ_{slow}^{inact}, are given in detail in Table 2.

the increased fraction of noninactivating current in E1537 mutant channels was caused by a combination of factors such as the relative decrease in the amplitude of the fast and calcium-dependent inactivation time constant, and the increase in the slower and Ba^{2+}-dependent inactivation time constant. The mutant slow inactivation time constants measured in Ca^{2+} were all significantly ($p < 0.01$) larger than the wild-type τ_{slow}^{inact}, whereas τ_{fast}^{inact} was not significantly different at the level $p < 0.1$. Furthermore, τ_{slow}^{inact} in Ca^{2+} and τ_{Ba}^{inact} in Ba^{2+} appeared remarkably similar for all calcium channel combinations and were found to increase in parallel in E1537Q, E1537S, E1537G, and E1537A channels. These observations suggest that mutations at position 1537 specifically affected the slow inactivation time constant in Ba^{2+} and Ca^{2+} solutions. As the inactivation time constant τ_{slow}^{inact} appeared to be independent of the charge carrier, there is a strong possibility that mutations at position 1537 modified the rate of the voltage-dependent transition to the inactivated state in α_{1C} channels. Assuming that voltage-dependent inactivation could proceed more rapidly from the open than from the closed state in $\alpha_{1C}/\alpha_{2b}/\beta_{2a}$ and $\alpha_{1C}/\alpha_{2b}/\beta_3$ channels, in sharp contrast to neuronal channels (Patil et al., 1998), τ_{slow}^{inact} in our experiments is likely to reflect changes in the rate of transition from the open to the inactivated state. It can always be argued that our whole-cell data could be explained as well by a faster open-to-closed transition or by a slower closed-to-open transition rate in E1537 mutant channels. However, any decrease in the channel open probability would also influence calcium-dependent inactivation unless Ca^{2+}-dependent and voltage-dependent inactivation proceeds from two distinct open states, as could happen in a modal kinetic model. Such a model has already been proposed to explain Ca^{2+}-dependent inactivation in L-type calcium channels (Imredy and Yue, 1994). At this stage, it can in any event be safely concluded that the apparent or macroscopic rate of Ba^{2+} inactivation has been modified in E1537 mutant channels.

Inactivation kinetics and whole-cell current density in E1537 mutant channels

Our first series of experiments clearly demonstrated that Ba^{2+} inactivation was significantly reduced in E1537 mutants as compared to inactivation in the wild-type channel. Whether these slower inactivation kinetics were primarily caused by an intrinsic change in the channel inactivation properties or rather were linked to a lower current density was further investigated in the following series of experiments. It is well established that calcium channel inactivation tends to process faster for larger currents. As whole-cell currents for the E1537 mutants were generally smaller than the wild-type currents recorded under the same conditions, the role of current density (or under our particular recording conditions, current amplitude) plays in conferring slower inactivation kinetics to E1537 mutants had to be carefully reviewed. The influence of peak current amplitude on E1537 channel inactivation was thus examined in Fig. 4. Whole-cell Ba^{2+} traces were recorded at the peak voltage for the wild-type, E1537Q, and E1537A channels, normalized and superimposed to magnify the differences in inactivation kinetics. As shown in Fig. 4 *A*, E1537A Ba^{2+} currents did not appreciably decay over the 450-ms voltage pulse to +10 mV, in contrast to wild-type Ba^{2+} currents. Whole-cell traces shown in the inset suggests that the rate of current activation may also be reduced in E1537A channels with, on average, $\tau_{act} = 3.8 \pm 0.7$ ms ($n = 12$) as compared to $\tau_{act} = 2.1 \pm 0.8$ ms ($n = 9$) for the wild-type channel. The permeation parameters were otherwise quite similar, as seen in the normalized *I-V* curve (Fig. 4 *B*) between the wild-type and the E1537A channel, because both activated around −25 mV and peaked at 0 mV. The E1537Q peaked at +10 mV in the presence of Ba^{2+}. Macroscopic *I-V* curves were also typically shifted to the right in the presence of Ca^{2+} for all channels (Fig. 4 *E*). For instance, the peak current shifted from 6 ± 2 mV ($n = 11$) in the presence of Ba^{2+} to 14 ± 1 mV ($n = 14$) in the presence of Ca^{2+} for the wild-type channel. This +8 mV shift was comparable to the shifts experimentally recorded for E1537Q (10 ± 0.5 mV to 19 ± 2 mV, $n = 11$) and E1537A (0 ± 0.5 mV to 6 ± 2 mV, $n = 14$) channels. The macroscopic current expression was generally higher for the wild-type channel as whole-cell Ba^{2+} currents averaged 1.3 ± 0.2 μA ($n = 11$), whereas E1537Q and E1537A generated smaller Ba^{2+} currents (see also Table 1). As seen in Fig. 4, *A* and *D*, Ba^{2+} and Ca^{2+} inactivation were not necessarily faster for larger currents. Two lines of evidence indeed suggest that whole-cell current amplitude was not the sole determinant in E1537 mutant slower inactivation kinetics. The first argument is circumstantial and pertains to the significant kinetic differences between E1537Q and E1537A, despite similar expression levels. Indeed, for all $V_m \geq 10$ mV, whole-cell Ba^{2+} and Ca^{2+} currents recorded for E1537Q were not significantly different in size than E1537A currents (Fig. 4, *C* and *F*), despite its slightly faster rate of inactivation. To circumvent the current density problem, we further designed a series of experiments whereby the relative ratio of the wild-type α_{1C} to the auxiliary subunits was progressively decreased such that wild-type α_{1C} currents would match the expression level of E1537 mutants. Alternatively, in a separate series of experiments, Ca^{2+} currents for the E1537 mutants were measured 4 days later than wild-type currents, hence increasing the probability of finding a mutant channel with Ca^{2+} currents comparable in size to those of the wild-type channel. The two approaches yielded similar results. As shown in Fig. 4 *D*, the superimposed yet not normalized whole-cell Ca^{2+} current traces measured at $V_m = +10$ mV for the wild-type, the E1537Q, and the E1537A channels yielded similar current amplitudes when recorded under the same experimental conditions. Despite generating a identical peak current of −0.66 μA, wild-type Ca^{2+} traces nonetheless inactivated significantly faster than E1537A traces, as only 15% of the wild-type currents remained at the end of the 450-ms pulse compared to 70% of the E1537A currents. Yet again, E1537Q currents displayed

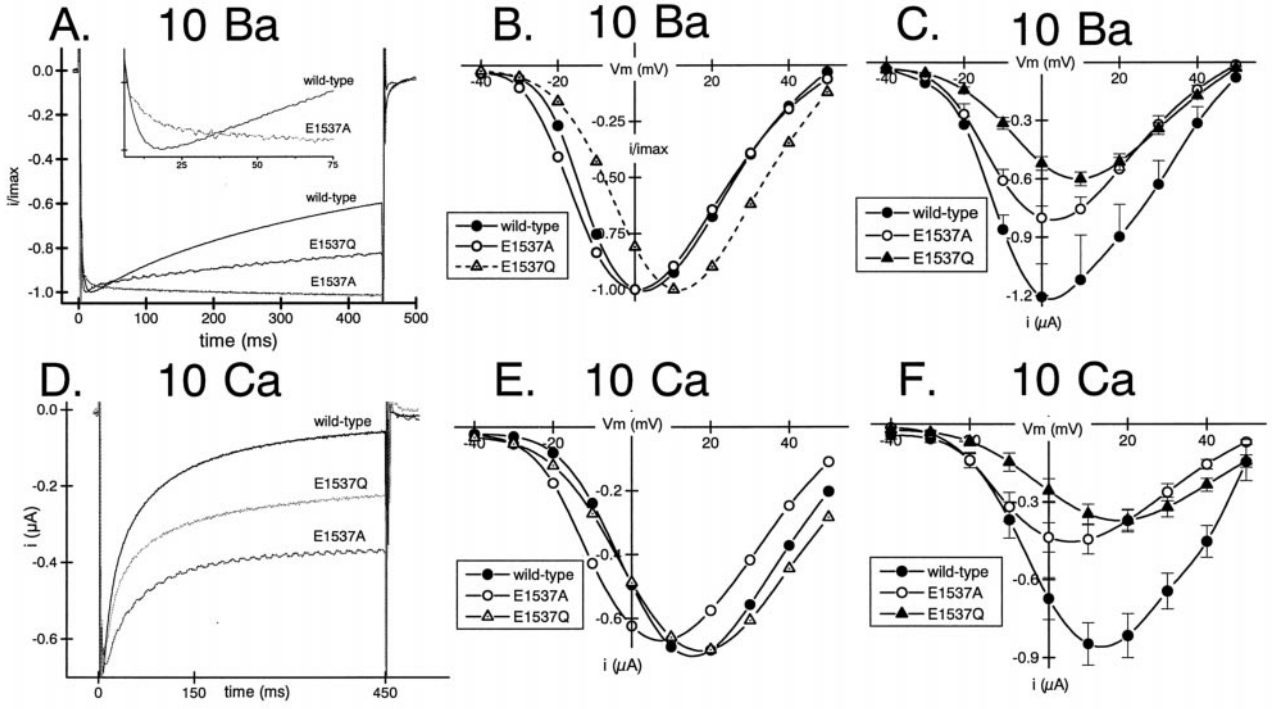

FIGURE 4 Whole-cell currents for wild-type $\alpha_{1C}/\alpha_{2b}\delta/\beta_{2a}$, E1537A/$\alpha_{2b}\delta/\beta_{2a}$, and E1537Q/$\alpha_{2b}\delta/\beta_{2a}$ channels were recorded in the presence of 10 mM Ba^{2+} (*upper panels*) and 10 mM Ca^{2+} (*lower panels*) by the pulse protocol previously described. (*A*) Whole-cell current traces recorded in the presence of 10 mM Ba^{2+} at +10 mV were normalized to 1.0 and superimposed. Ba^{2+} inactivation was faster for wild-type > E1537Q > E1537A channels. As shown in the insert, the E1537A activation also appeared to be noticeably slower. (*B*) The corresponding normalized *I-V* curves obtained in the presence of 10 mM Ba^{2+} are shown. The wild-type and E1537A current-voltage curves peaked at 0 mV, whereas the E1573Q channel peaked at +10 mV. On average, *I-V* curves peaked at the following voltages: 6 ± 2 mV ($n = 11$) for the wild-type $\alpha_{1C}/\alpha_{2b}\delta/\beta_{2a}$, 0 ± 0.4 mV ($n = 15$) for E1537A/$\alpha_{2b}\delta/\beta_{2a}$, and 10 ± 1 mV ($n = 14$) for E1537Q/$\alpha_{2b}\delta/\beta_{2a}$ channels. (*C*) Ba^{2+} whole-cell current amplitude was higher on average for the wild-type channel with a peak current of 1.2 ± 0.1 μA ($n = 11$) as compared to peak currents of 0.81 ± 0.06 μA ($n = 15$) for E1537A/$\alpha_{2b}\delta/\beta_{2a}$ and 0.63 ± 0.04 μA ($n = 14$) for E1537Q/$\alpha_{2b}\delta/\beta_{2a}$ channels. For clarity, only the positive error bars are shown for the wild-type channel. (*D*) Whole-cell currents obtained in 10 mM Ca^{2+} are shown superimposed at $V_m = 10$ mV. Current traces were not normalized because in that particular case, wild-type $\alpha_{1C}/\alpha_{2b}\delta/\beta_{2a}$, E1537A/$\alpha_{2b}\delta/\beta_{2a}$, and E1537Q/$\alpha_{2b}\delta/\beta_{2a}$ channels yielded whole-cell Ca^{2+} currents in the same range. As seen, wild-type α_{1C} Ca^{2+} currents were typically faster than E1537A Ca^{2+} currents, independently of the whole-cell current amplitude. E1537Q channels yielded current traces with an intermediate inactivation time course. (*E*) Corresponding *I-V* curves. As expected, whole-cell Ca^{2+} *I-V* curves are shifted to the right. Wild-type and E1537Q Ca^{2+} currents peaked, respectively, at $V_m = 14 \pm 1$ mV ($n = 14$) and 19 ± 3 mV ($n = 11$), whereas E1537A Ca^{2+} currents peaked at $V_m = 5 \pm 1$ mV ($n = 14$). (*F*) Whole-cell Ca^{2+} current amplitude was higher on average for the wild-type channel with a peak current of 0.61 ± 0.08 μA ($n = 14$) as compared to peak currents of 0.43 ± 0.05 μA ($n = 14$) for E1537A/$\alpha_{2b}\delta/\beta_{2a}$ and 0.27 ± 0.04 μA ($n = 11$) for E1537Q/$\alpha_{2b}\delta/\beta_{2a}$ channels.

an intermediate rate of inactivation, with 38% noninactivating currents. Results obtained in Fig. 4 *D* thus minimized the possible role of current-dependent inactivation in the slower inactivation kinetics of E1537 mutants. From Fig. 4 it also appears that the current time course measured in Ca^{2+} solutions was qualitatively similar for all channels. As the curve fitting analysis demonstrated, the major kinetic effect brought about by Ca^{2+} is seen in an additional inactivation time constant that is relatively fast, τ_{fast}^{inact}, and was absent in Ba^{2+} traces. This faster inactivation time constant τ_{fast}^{inact} remained present in all mutant channels, furthering the notion that calcium-dependent inactivation was not specifically modified in E1537 mutant channels.

Voltage dependence of the E1537A inactivation time constants

In voltage-dependent ion channels, voltage controls kinetic transitions, and more specifically, positive voltage encourages transitions from the closed to the open state, and ultimately to the inactivated state. Thus in a traditional model of voltage-dependent inactivation where inactivation is strongly coupled to the open state, inactivation is expected to speed up with membrane depolarization (Armstrong and Bezanilla, 1977; Bean, 1981; Imredy and Yue, 1994). Mutations at E1537 can lead to a slower inactivation by one of the following mechanisms, either by slowing the macroscopic rate of transition to the inactivated state or by making the channel unresponsive to membrane depolarization. We thus investigated the influence of voltage on the inactivation time constants for the E1537A mutant channel. Inactivation time constants for the wild-type $\alpha_{1C}/\alpha_{2b}\delta/\beta_{2a}$ and E1537A/$\alpha_{2b}\delta/\beta_{2a}$ channels were estimated at time $t = 2$ s and reported as a function of the applied membrane potential between −10 and +20 mV (Fig. 5). As seen in the left panel, τ_{Ba}^{inact} for the wild-type channel decreased from 918 ± 43 ms to 627 ± 46 ms ($n = 7$) between −10 and +20 mV; hence membrane depolarization appeared to

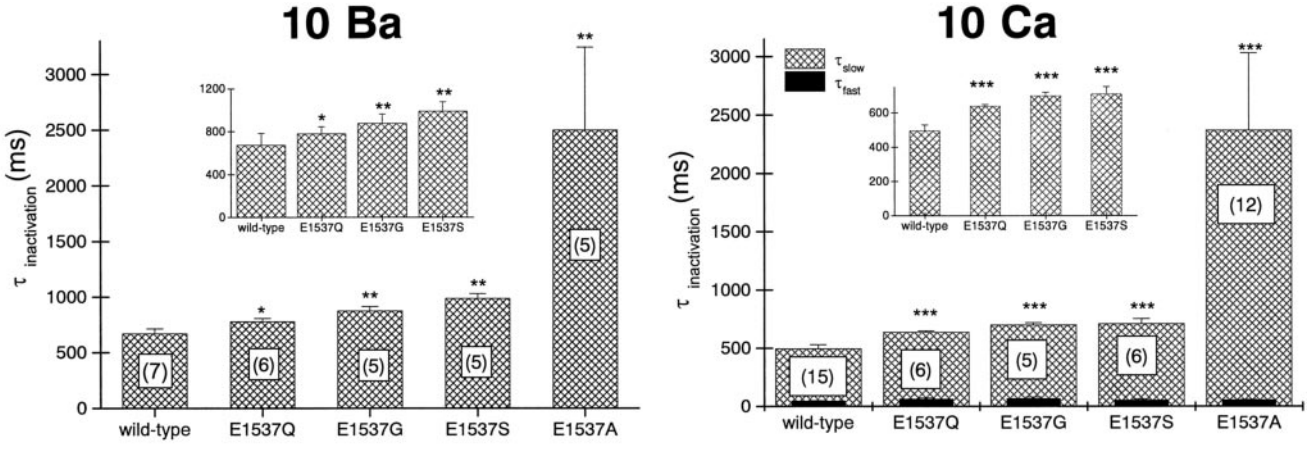

FIGURE 5 Inactivation time constants for the wild-type $\alpha_{1C}/\alpha_{2b}\delta/\beta_{2a}$ and E1537A/$\alpha_{2b}\delta/\beta_{2a}$ channels were estimated between time $t = 0$ and time $t = 2$ s and reported as a function of the applied membrane potential between -10 and $+20$ mV. (*Left*) For the wild-type Ba^{2+} traces, the inactivation time constants decreased from 918 ± 43 ms to 627 ± 46 ms ($n = 7$) between -10 and $+20$ mV; hence membrane depolarization appeared to speed up inactivation in the presence of Ba^{2+}. In contrast, the E1537A inactivation time constants increased at least threefold over the same voltage range with $\tau_{Ba}^{inact} = 1221 \pm 246$ ms at -10 mV to 3609 ± 1329 ms ($n = 5$) at $+20$ mV. Note that the inactivation time constants estimated at -10 mV are not significantly different for the wild-type and the E1537A channel. (*Right*) The Ca^{2+} inactivation time course can best be fitted with two exponential functions. Again, the fast Ca^{2+} inactivation time constant is not significantly different between the wild-type and the E1537A channel, with τ_{fast}^{inact} ranging from 41 ± 5 ms to 73 ± 5 ms ($n = 7$) for the wild-type channel and 49 ± 3 ms to 69 ± 4 ms ($n = 10$) for E1537A. In contrast, the slow Ca^{2+} inactivation time constant τ_{slow}^{inact} was consistently higher for E1537A than for wild-type α_{1C} channels at all membrane potentials. For the wild-type channel, τ_{slow}^{inact} decreased from 732 ± 7 ms to 521 ± 51 ms ($n = 7$), whereas τ_{slow} actually increased from 990 ± 99 ms to 1823 ± 115 ms ($n = 10$) between -10 and $+20$ mV. Thus the E1537A channel appeared to become slower in response to membrane depolarization in both Ba^{2+} and Ca^{2+} solutions.

speed up inactivation in the presence of Ba^{2+}. This observation has previously been reported for native L-type calcium currents in isolated myocytes from adult rat (Imredy and Yue, 1994) when it was shown that the decay of Ba^{2+} currents accelerates monotonically with depolarization. In contrast, the E1537A inactivation time constants increased at least threefold over the same voltage range, with τ_{Ba}^{inact} increasing from 1221 ± 246 ms at -10 mV to 3609 ± 1329 ms ($n = 5$) at $+20$ mV. Note that the inactivation time constants estimated at -10 mV were not significantly different for the wild-type and the E1537A channel. Similar results were obtained for τ_{slow}^{inact} in Ca^{2+} solutions. Moreover, the slow inactivation time constants between Ba^{2+} and Ca^{2+} turn out to be remarkably similar between -10 and $+20$ mV for wild-type and mutant channels. The apparent similarity between τ_{Ba}^{inact} and τ_{slow}^{inact} in Ca^{2+} argues that the mutations are primarily affecting an inactivation path present in both Ba^{2+} and Ca^{2+} solutions. As seen previously in Fig. 3, τ_{fast}^{inact} was not significantly different between the wild-type and the E1537A channel, with τ_{fast}^{inact} ranging from 41 ± 5 ms to 73 ± 5 ms ($n = 7$) for the wild-type channel and from 49 ± 3 ms to 69 ± 4 ms ($n = 10$) for E1537A. In contrast, τ_{slow}^{inact} in Ca^{2+} was consistently higher for E1537A than for wild-type α_{1C} channels at all membrane potentials. For the wild-type channel, τ_{slow}^{inact} decreased from 732 ± 7 ms to 521 ± 51 ms ($n = 7$), whereas in E1537A channels, τ_{slow}^{inact} actually increased from 990 ± 99 ms to 1823 ± 115 ms ($n = 10$) between -10 and $+20$ mV. Thus, not only was the E1537A channel slower at all membrane potentials than the wild-type channel; it also appeared to become slower with membrane depolarization in both Ba^{2+} and Ca^{2+} solutions.

Isochronic inactivation measurements in Ba^{2+} and Ca^{2+} for E1537 mutant channels

To provide a more quantitative picture of barium- and calcium-dependent inactivation in E1537 mutant channels, we performed a series of isochronic inactivation experiments at time $t = 5$ s. In such experiments, the relative amplitude of the tail currents, measured at the test pulse of $+10$ mV, is proportional to the number of channels present in the open state at that given time or inversely proportional to the number of channels present in the inactivated state. From the relationship between the current amplitude and the conditioning voltage, one can extract "steady-state" information such as the voltage range where channels are experiencing inactivation. Isochronic inactivation data thus provide a snapshot picture of the channel inactivation properties unhampered by time-dependent factors. To achieve inactivation measurements in the absence of kinetic variations, conditioning pulses should be, in theory, many times longer than the slower inactivation time constant. For α_{1C} calcium channels, these considerations, however, must take into account the slow but irreversible time-dependent rundown associated with whole-cell experiments. Hence, our Ba^{2+} isochronic inactivation experiments with 5-s conditioning pulses are not true "steady-state" experiments, but may provide valuable insight into the inactivation process. In the presence of Ba^{2+}, the voltage dependence of 5-s isochronic inactivation was inves-

tigated for the wild-type $\alpha_{1C}/\alpha_{2b}\delta/\beta_{2a}$, E1537Q/$\alpha_{2b}\delta/\beta_{2a}$, E1537S/$\alpha_{2b}\delta/\beta_{2a}$, E1537G/$\alpha_{2b}\delta/\beta_{2a}$, and E1537A/$\alpha_{2b}\delta/\beta_{2a}$ channels. Fig. 6 shows the whole-cell current traces recorded for wild-type $\alpha_{1C}/\alpha_{2b}\delta/\beta_{2a}$ and E1537A/$\alpha_{2b}\delta/\beta_{2a}$ channels by the tripulse protocol shown, in the presence of 10 mM Ba^{2+} (*upper panel*) and 10 mM Ca^{2+} (*lower panel*). The fraction of noninactivated whole-cell current remaining at the end of the 5-s pulse was measured at the test pulse of +10 mV (peak voltage), which was then plotted against the prepulse voltage. Pooled fractional currents shown in the extreme right panels were fitted to a Boltzmann equation (Eq. 1). In the presence of 10 mM Ba^{2+}, 67 ± 2% (n = 9) of the wild-type channels were completely inactivated by a 5-s pulse to +10 mV. In contrast, only 11 ± 4% (n = 6) of the E1537A channels were completely inactivated under the same conditions. The E1537A inactivation in Ba^{2+} was so shallow that it could not be approximated by Boltzmann functions. The other mutant channels showed intermediate steady-state inactivation properties with a fractional inactivation of 42 ± 3% (n = 11) for E1537Q, 39 ± 3% (n = 3) for E1537S, and 42 ± 2% (n = 4) for E1537S channels. The fitted Boltzmann parameters and the corresponding estimated fit errors are given in the figure legend. In contrast to the Ba^{2+} data, Ca^{2+}-induced inactivation appeared to proceed almost to completion for all channel combinations. After a 5-s voltage pulse of +10 mV, whole-cell wild-type currents were inactivated at 83 ± 5% (n = 11), as compared to 75 ± 2% (n = 4) of the E1537Q currents, 80 ± 1% (n = 4) of the E1537G currents, and 81 ± 5% (n = 4) of

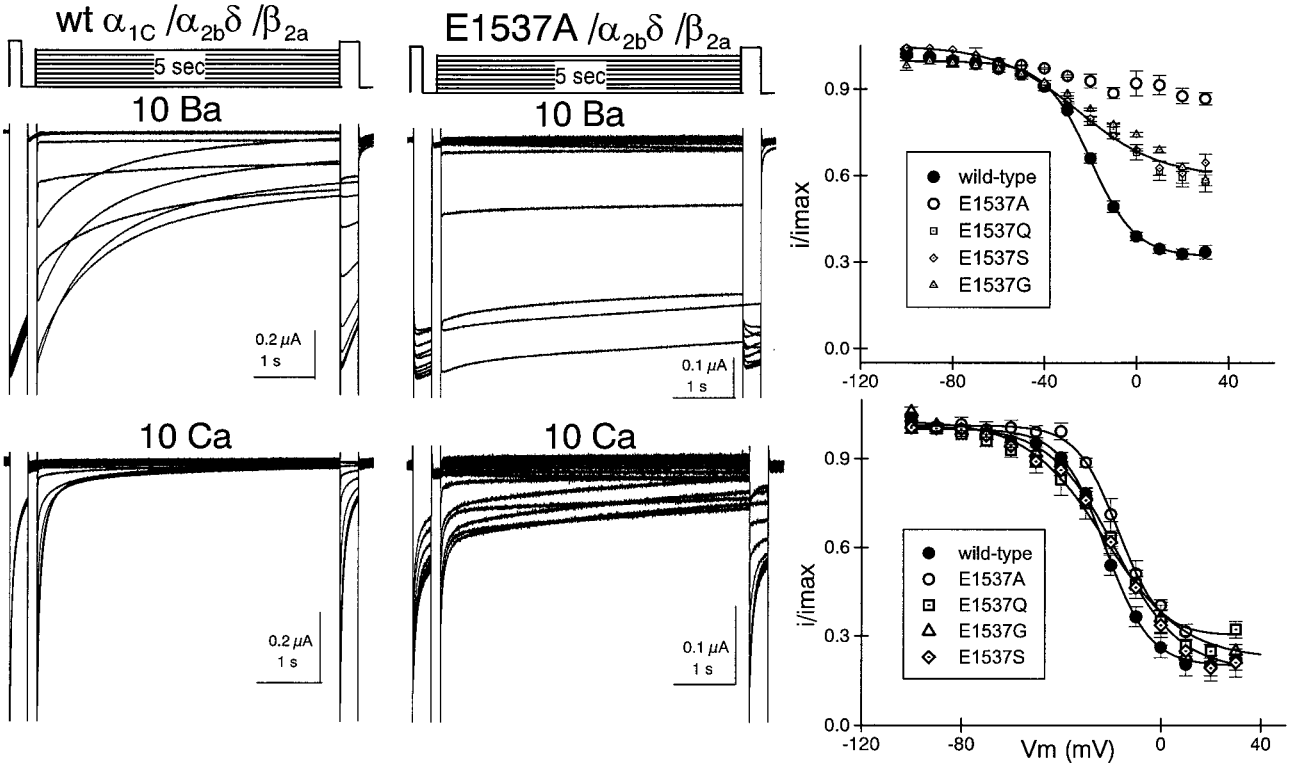

FIGURE 6 The voltage dependence of inactivation was investigated for the wild-type $\alpha_{1C}/\alpha_{2b}\delta/\beta_{2a}$, E1537Q/$\alpha_{2b}\delta/\beta_{2a}$, E1537S/$\alpha_{2b}\delta/\beta_{2a}$, E1537G/$\alpha_{2b}\delta/\beta_{2a}$, and E1537A/$\alpha_{2b}\delta/\beta_{2a}$ channels at the end of a 5-s prepulse. The inactivation protocol is shown on top of the whole-cell recordings. Holding potential was −80 mV, the test voltage was the peak voltage (usually around 0 mV in Ba^{2+} and +10 mV in Ca^{2+}), and 14 prepulses were applied from −100 to +30 mV, by 10-mV steps at a frequency of 0.05 Hz. Acquisition frequency was 2 kHz. Inactivation was measured in the presence of 10 mM Ba^{2+} (*top traces*) and in the presence of 10 mM Ca^{2+} (*bottom traces*) after BAPTA injection. The fraction of the noninactivating current was recorded at the end of the 5-s pulse and reported on the steady-state inactivation curve shown at the right. Only the whole-cell current traces obtained with the wild-type and the E1537A channels are shown. (*Upper right*) In the presence of 10 mM Ba^{2+}, 67 ± 2% (n = 9) of the wild-type (●) channels were completely inactivated at the end of a 5-s pulse to +10 mV. In contrast, only 11 ± 4% (n = 6) of the E1537A channels (○) were completely inactivated under the same conditions. Other mutant channels showed intermediate steady-state inactivation properties with fractional inactivation of 42 ± 3% (n = 11) for E1537Q, 39 ± 3% (n = 3) for E1537S, and 42 ± 2% (n = 4) for E1537S channels. Inactivation data were pooled from independent experiments performed on single oocytes and fitted to Boltzmann functions, using the following fit parameters and the corresponding estimated fit errors (Eq. 1): z = 2.4 ± 0.2, $E_{0.5}$ = −20 ± 0.7 mV (wild-type); z = 1.4 ± 0.1, $E_{0.5}$ = −18 ± 2 mV (E1537Q), z = 1.2 ± 0.2, $E_{0.5}$ = −19 ± 1 mV (E1537S); z = 1.3 ± 0.1, $E_{0.5}$ = −17 ± 2 mV (E1537G). The E1537A inactivation data point could not be approximated by Boltzmann functions. (*Lower right*) Inactivation was almost complete at the end of a 5-s prepulse in the presence of 10 mM Ca^{2+}. At +10 mV, whole-cell wild-type currents (●) were inactivated at 83 ± 5% (n = 11), as compared to the inactivation level of 75 ± 2% (n = 4) for the E1537Q currents (⊡), 80 ± 1% (n = 4) for E1537G (△), 81 ± 5% (n = 4) for E1537S (◇). With its inactivation level of 69 ± 3% (n = 7), E1537A inactivation data points were almost indistinguishable from the wild-type and other E1537 mutants. In the presence of Ca^{2+}, inactivation data points were typically bell shaped for the wild-type and mutant channels alike, but these points were omitted for the sake of clarity. The fit parameters were z = 2.8 ± 0.2 and $E_{0.5}$ = −22 ± 1 mV (wild-type); z = 1.9 ± 0.2 and $E_{0.5}$ = −18 ± 2 mV (E1537G); z = 1.9 ± 0.2 and $E_{0.5}$ = −16 ± 1 mV (E1537S); z = 1.6 ± 0.4 and $E_{0.5}$ = −22 ± 3 mV (E1537Q); z = 3.0 ± 0.3 and $E_{0.5}$ = −17.0 ± 0.7 mV (E1537A).

the E1537S currents. With a inactivation level of 69 ± 3% ($n = 7$), E1537A yielded inactivation data points in Ca^{2+} that were almost indistinguishable from the wild-type and other E1537 mutants. Isochronic inactivation experiments performed at a shorter time, $t = 2$ s, proved to be qualitatively similar, with the exception that inactivation was somewhat reduced in E1537A channels with 49 ± 3% ($n = 3$) (results not shown). Remarkably, inactivation in the presence of Ca^{2+} ensued to a similar extent for all channels, despite the slower Ba^{2+} inactivation in E1537 mutant channels. This suggests again that E1537 mutations altered the slow voltage-dependent transition to the inactivated state without affecting the faster calcium-dependent inactivation. Hence voltage-dependent and calcium-dependent inactivation could involve a series of seemingly independent transitions (Hadley and Lederer, 1991) from kinetically similar closed and open states. Alternatively, voltage-dependent transitions could occur all together in a gating mode parallel to calcium-facilitated ones, as has previously been suggested in the Ca^{2+}-induced gating shift model (Imredy and Yue, 1994).

In summary, E1537 mutations significantly reduced Ba^{2+}-dependent inactivation. Inactivation proceeded more completely for hydrophilic residues such as glutamate, but was least complete for the hydrophobic residues such as alanine. Five-second pulses to positive membrane potentials in Ba^{2+} failed to inactivate more than 15% of the E1537A channels, in contrast to ~70% of the wild-type channels. These huge differences collapsed in the presence of Ca^{2+}, where inactivation proceeded almost to completion for wild-type and mutant channels alike, with 70–85% of calcium currents inactivated after a 5-s pulse. Hence Ca^{2+} preserved its dominant role in the inactivation kinetics of the cardiac α_{1C} wild-type and E1537 mutant channels.

DISCUSSION

E1537 mutations slow macroscopic inactivation of Ca^{2+} channels

In cardiac L-type calcium channels, inactivation proceeds through the combined effect of voltage and calcium ions (Kass and Sanguinetti, 1984; Lee et al., 1985; Campbell et al., 1988; Imredy and Yue, 1994), although Ca^{2+}-facilitated inactivation arises as the prominent inactivation mechanism under physiological conditions. We have investigated herein the role of E1537 located in the EF-hand binding motif of the cardiac α_{1C} channel in calcium channel inactivation kinetics. Mutant channels E1537Q, E1537S, E1537G, and E1537A were found to display significantly slower inactivation kinetics in Ba^{2+} and Ca^{2+} solutions. Whole-cell Ba^{2+} and Ca^{2+} currents were found to proceed more slowly as the E residue was replaced by hydrophobic residues in the following order: E > Q > G ≈ S > A. Slower kinetics can indeed be readily observed in Ba^{2+} solutions. Hence our results show that point mutations in the proximal part of the C-terminus may additionally impair Ba^{2+}-dependent inactivation rather than intrinsically modifying Ca^{2+}-dependent inactivation. The result that mutations at E1537 could alter Ba^{2+}-dependent inactivation was quite unexpected, as this region is known to be involved in calcium-dependent inactivation. Alanine substitution was most crucial in that regard, with a fourfold increase in τ_{Ba}^{inact} in Ba^{2+} and τ_{slow}^{inact} in Ca^{2+} as compared to the wild-type α_{1C} channel.

Over the years, Ba^{2+} solutions have typically been used to assess voltage-dependent inactivation in L-type calcium channels (Kass and Sanguinetti, 1984; Campbell et al., 1988). More recent observations, however, revealed that ion-dependent inactivation may subsist in the presence of Ba^{2+} in some L-type and non-L-type calcium channels (Ferreira et al., 1997; Parent et al., 1997; Forsythe et al., 1998). By definition, pure voltage-dependent inactivation should proceed unimpaired in the complete absence of divalent cations, with either Na^+ or Li^+ as the charge carrier. Thus the Ba^{2+} data reported in this paper cannot be equated a priori with a true measure of voltage-dependent inactivation in α_{1C} channel and mutants. A few lines of evidence suggest, however, that in this series of experiments, Ba^{2+} inactivation could represent a fair approximation of voltage-dependent inactivation. First, as seen in Fig. 5, the slow inactivation time constants between Ba^{2+} and Ca^{2+} turned out to be remarkably similar between −10 and +20 mV for wild-type and mutant channels. The apparent similarity between τ_{Ba}^{inact} and τ_{slow}^{inact} in Ca^{2+} solutions argues that the mutations are probably primarily affecting a inactivation path present in both Ba^{2+} and Ca^{2+} solutions. Such a gating transition could thus be identified as the voltage-dependent transition to the inactivated state, because voltage-dependent inactivation remains in Ca^{2+} solutions. Our kinetic analysis further suggests that the overall Ba^{2+} kinetics probably result mostly from an impaired voltage-dependent inactivation, as the voltage-dependent time constants for E1537 mutants increased rather than decreased, in response to membrane depolarization (see Fig. 5). The impaired voltage-dependent inactivation in E1537 mutant channels could thus be said to be responsible for the overall slower inactivation kinetics in Ba^{2+} as well as in Ca^{2+} solutions. Hence, although E1537 mutant channels displayed overall slower inactivation under the same conditions as the wild-type α_{1C} channel, their fast Ca^{2+}-dependent inactivation time constant (τ_{fast}^{inact}) remained relatively constant. Ca^{2+}-dependent inactivation remained typically and significantly faster than Ba^{2+} inactivation kinetics for all channels, mutants and wild-type alike. Ca^{2+} inactivation that is faster than Ba^{2+} inactivation remains the trademark of calcium-dependent inactivation, typically observed in genuine L-type α_{1C} calcium channels. The conclusion that Ca^{2+}-dependent inactivation was preserved in E1537 mutants was supported by isochronic inactivation measurements at time $t = 2$ s and $t = 5$ s. Roughly 70–85% of the wild-type and mutant channels alike were inactivated by sustained depolarization in Ca^{2+} solutions. Our observations that the E1537 mutations failed to abolish calcium-dependent inactivation but yielded slower inactivating channels agree with the study of the α_{1C} triple mutant D1535A +

E1537A + D1546A (Zhou et al., 1997). The triple mutant failed to abolish calcium-dependent inactivation, although the Ca^{2+} current traces they recorded from the α_{1C} triple mutant (D1535A + E1537A + D1546A) were actually twice as slow as the ones recorded for the wild-type channel. Point mutations in the EF-hand binding motif thus appear to impair α_{1C} calcium channel inactivation, but not solely Ca^{2+}-dependent inactivation.

The picture provided by the isochronic inactivation analysis could be satisfactorily explained by the Ca^{2+}-induced modal gating mechanism proposed by Imredy and Yue (1994). Whereas in practice, voltage-gated channels are represented by a linear activation scheme, L-type calcium channels appear to activate through two parallel gating modes in the presence of Ca^{2+}. Thus Ca^{2+} entry through the channel appears to promote a gating shift toward mode 0 or mode Ca, characterized by infrequent openings, whereas mode 1 would predominate in the presence of Ba^{2+}. In this gating model, Ca^{2+}-sensitive inactivation could destabilize the open state without appreciably interfering with voltage dependence transitions. This gating model predicts a clear separation between Ca^{2+} and voltage-dependent inactivation in Ca^{2+} channels. Mechanistically, our results could be explained by the presence of these two parallel activation schemes, one Ca^{2+} modified and the other unmodified, which would be in rapid equilibrium. In the presence of Ca^{2+}, transitions from the open to the inactivated state may proceed through a voltage-dependent pathway or a calcium-facilitated one. E1537 mutations appear to selectively modify the rate of voltage-dependent transitions in mode 1, leaving the Ca^{2+}-dependent transitions in mode 0 relatively untouched. Hence, in the presence of Ca^{2+}, most channels (wild-type and mutants alike) would reach the inactivated state after a long depolarization pulse ($t > 2$ s), regardless of the rate of inactivation through voltage-dependent steps. The structure-function data gathered in our study thus provide additional support for the postulate that voltage-dependent inactivation and calcium-dependent inactivation occur independently, as suggested before (Hadley and Lederer, 1991; Obejero-Paz et al., 1991; Imredy and Yue, 1994).

Locus of calcium-dependent inactivation

Structure-function studies on calcium-dependent inactivation have recently attracted a lot of attention. Most groups have chosen the chimeric approach by studying the inactivation properties of α_{1C}-α_{1E} chimeric constructs (DeLeon et al., 1995; Zhou et al., 1997) and α_{1C}-α_{1S} chimera (Adams and Tanabe, 1997), whereas another group opted for systematic deletions of the human fibroblast L-type $\alpha_{1C,77}$ isoform (Soldatov et al., 1997; Zühlke and Reuter, 1998). First in line, the group of David Yue suggested that the EF-hand binding motif located in the C-terminus of α_{1C} might be responsible for calcium-dependent inactivation in α_{1C} channels (DeLeon et al., 1995). Indeed, Ca^{2+}-dependent inactivation appeared to be eliminated when the EF-hand binding motif and some surrounding residues were replaced by the corresponding region of α_{1E}. The calcium sensitivity factor f used in their study was estimated from the ratio of Ca^{2+} to Ba^{2+} peak currents, as measured at time $t = 300$ ms. When a similar analysis was applied to our E1537 mutant data, we found that the calcium sensitivity factor f would decrease somewhat from the wild-type to the E1537A channel from 0.68 ± 0.09 ($n = 4$) to the nonzero value of 0.41 ± 0.03 ($n = 5$). As the calcium sensitivity factor had decreased in our mutants, we first concluded that calcium-dependent inactivation alone had been modified (Porter Moore et al., 1997). As it turned out, isochronic inactivation data measured at 5 s (see Fig. 6) indicate that E1537 mutations affected Ba^{2+} inactivation to a greater extent than Ca^{2+}-dependent inactivation. As explained earlier, assuming that Ba^{2+}-dependent inactivation reflects to some extent voltage-dependent inactivation in α_{1C} calcium channels, reduced voltage-dependent inactivation would result in slower inactivation in Ba^{2+} and Ca^{2+} solutions. However, we cannot exclude a small effect on calcium-dependent inactivation, as the extent of "steady-state" calcium-dependent decreased slightly from 85% to 70% from the wild-type to the E1537A mutant.

Because there are in fact only a few nonconserved substitutions in the respective EF-hand motifs of the cardiac α_{1C} and the brain α_{1E} subunits, Zhou and colleagues (1997) made triple point mutations in the α_{1C} backbone. Furthermore, by carefully measuring inactivation time constants on α_{1C}-α_{1E} chimeric channels, Zhou and colleagues (1997) came to the conclusion that a segment of ~200 AA downstream from the EF-hand binding motif was more critical than the sum of the D1535 + E1537 + D1546 residues present in the EF-hand motif itself. Last, the skeletal α_{1S} subunit, which is identical to α_{1C} in the EF-hand region, does not experience typical calcium-dependent inactivation, at least in native membranes (Mejia-Alvarez et al., 1991). Thus, in retrospect, it may not be too surprising to find that mutations in the EF-hand motif of the α_{1C} subunit failed to abolish calcium-dependent inactivation (Zhou et al., 1997; our results). The current consensus in this matter raises the possibility that calcium-dependent inactivation involves many cytoplasmic sites of the α_{1C}, with portions of the C-terminus being major players (Zhou et al., 1997; Adams and Tanabe, 1997; Zühlke and Reuter, 1998). Needless to say, the identification of the C-terminus as a possible locus for calcium-dependent inactivation in α_{1C} agrees satisfactorily with the autoinhibition model developed by Imredy and Yue (1992), whereby calcium influx through a given channel causes calcium-dependent inactivation of the same channel. Moreover, based on the observation that injection of BAPTA in *Xenopus* oocytes does not interfere with calcium-dependent inactivation, the inhibitory site for Ca^{2+} should be very close to the channel inner mouth or even in the channel pore itself, according to a recent kinetic analysis of α_{1C}/β_{2a} channels (Noceti et al., 1998). All together, these observations could be explained with a model whereby Ca^{2+} binding to the distal part of the C-terminus produces

a conformational change that would then enable it to block the channel pore. The tertiary structure of voltage-dependent calcium channels may be needed to definitively reconcile the current structure-function data on calcium-dependent inactivation. The ongoing speculation about the molecular determinants of Ca^{2+}-induced inactivation highlights the intricate and complex nature of this mechanism that may involve more than a single site.

Locus of voltage-dependent inactivation

The mutations at position 1537 in α_{1C} mutant channels appeared to disrupt voltage-dependent inactivation, as measured in Ba^{2+} solutions. The suggestion that the C-terminus may play a role in the voltage-dependent inactivation of α_{1C} channels was quite unexpected. Previous work with chimeric channels led to the conclusion that voltage-dependent inactivation involves residues surrounding S6 in repeat I (Zhang et al., 1994; Parent et al., 1995) or residues located in the intracellular linker connecting repeats I and II (Herlitze et al., 1997). In the absence of a definitive molecular model, calcium channel inactivation could be analyzed in terms of the mechanisms accounting for inactivation in voltage-dependent K^+ and Na^+ channels. In fact, some features of calcium channel inactivation, most notably the role of pore I, may be reminiscent of slow C-type inactivation in K^+ channels that depends strongly on residues located in the channel pore and in the channel extracellular mouth (Lòpez-Barneo et al., 1993; Liu et al., 1996; Kiss and Korn, 1998). However, the prototypical model for voltage-dependent inactivation remains the "ball-and-chain model," first designed to account for fast voltage-dependent inactivation in Na^+ channels (Armstrong and Bezanilla, 1977). To this date, it remains to be seen whether the ball-and-chain model can also aptly describe calcium channel inactivation. In voltage-dependent K^+ and Na^+ channels, the main structural determinants for fast inactivation were found to be, respectively, the N-terminus and the III–IV linker (Hoshi et al., 1990; West et al., 1992). These tethered plugs located on the cytoplasmic face of the channel are believed to move toward the channel inner mouth in response to membrane depolarization. By locking themselves onto the channel mouth, the tethered balls could thus effectively prevent ion fluxes through the channel. At this time, the possibility that the IS6 residues in Ca^{2+} channels could contribute to a receptor site for a tethered plug such as the one present in the ball-and-chain model cannot be excluded. Nonetheless, the molecular identity of a possible intracellular tethered ball in voltage-dependent calcium channels remains elusive, despite the report that intracellular application of trypsin selectively removed voltage-dependent inactivation in L-type calcium channels (Obejero-Paz et al., 1991; Klockner et al., 1995). In view of the results described in our study, we could speculate that part of the intracellular C-terminus close to IVS6, including some residues of the EF-hand binding motif, may carry out the role of the inactivation ball in the α_{1C} channel. Many conflicting observations would remain unexplained by our working hypothesis, however. Intracellular application of trypsin was also found to disrupt calcium-dependent inactivation (You et al., 1995). Furthermore, the distal part of the C-terminus, encompassing the same region recently implicated in calcium-dependent inactivation, was identified as carrying the effect of trypsin on the voltage-dependent inactivation of calcium channels (Klockner et al., 1995). Last, it would also be difficult to generalize this working hypothesis to other calcium channels. As it was pointed out in Fig. 1, the α_{1A}, α_{1B}, and α_{1E} calcium channels all display alanine residues at the corresponding position, yet there is no doubt that the α_{1E} channel at least undergoes fast Ba^{2+} inactivation kinetics (Parent et al., 1997). These problems and discrepancies illustrate the difficulty of studying structure-function relationships with regard to calcium channel inactivation. From that perspective, our results may serve as a reminder that although voltage-dependent inactivation and calcium-dependent inactivation happen as kinetically distinct events, their molecular identification has yet to be clearly established in voltage-dependent calcium channels.

We thank Dr. Terry P. Snutch for the rat brain $\alpha_{2b}\delta$ subunit, Dr. Ed Perez-Reyes for the β_{2a} subunit, J. Verner and B. Wallendorff for skilled oocyte injection, C. Porter Moore for preliminary experiments, Dr. R. Sauvé for discussions, and Dr. Kurt G. Beam for comments.

This work was initiated with National Institutes of Health I grant R29-HL54708 and was completed with grants from the Medical Research Council of Canada, the "Fonds de la Recherche en Santé du Québec," and the Canadian Heart and Stroke Foundation to LP.

REFERENCES

Adams, B., and T. Tanabe. 1997. Structural regions of the cardiac Ca channel α_{1C} subunit involved in Ca-dependent inactivation. *J. Gen. Physiol.* 110:379–389.

Armstrong, C. M., and F. Bezanilla. 1977. Inactivation of the sodium channel. II. Gating current experiments. *J. Gen. Physiol.* 70:567–590.

Babitch, J. 1990. Channel hands "letter." *Nature.* 346:321–322.

Bean, B. P. 1981. Sodium channel inactivation in the crayfish giant axon. *Biophys. J.* 35:595–614.

Campbell, D. L., W. R. Giles, J. R. Hume, and E. F. Shibata. 1988. Inactivation of calcium current in bull-frog atrial myocytes. *J. Physiol. (Lond.).* 403:287–315.

Cannell, M. B., H. Cheng, and W. J. Lederer. 1995. The control of calcium release in heart muscle. *Science.* 268:1045–1049.

Castellano, A., X. Wei, L. Birnbaumer, and E. Perez-Reyes. 1993. Cloning and expression of a third calcium channel β subunit. *J. Biol. Chem.* 268:3450–3455.

Creighton, T. E. 1993. Proteins, Structures and Molecular Properties. W. H. Freeman and Company, New York.

daSilva, J. J. R. F., and R. J. P. Williams. 1993. The Biological Chemistry of the Elements. Clarendon Press, Oxford.

DeLeon, M., Y. Wang, L. Jones, E. Perez-Reyes, X. Wei, T. W. Soong, T. P. Snutch, and D. T. Yue. 1995. Essential Ca^{2+}-binding motif for Ca^{2+}-sensitive inactivation of L-type Ca^{2+} channels. *Science.* 270: 1502–1506.

DeWaard, M., and K. P. Campbell. 1995. Subunit regulation of the neuronal α_{1A} Ca^{2+} channel expressed in *Xenopus* oocytes. *J. Physiol. (Lond.).* 485:619–634.

Ferreira, G., J. Yi, E. Ríos, and R. Shirokov. 1997. Ion-dependent inactivation of barium current through L-type calcium channels. *J. Gen. Physiol.* 109:449–461.

Forsythe, I. D., T. Tsujimoto, M. Barnes-Davies, M. Cuttle, and T. Takahashi. 1998. Inactivation of presynaptic calcium current contributes to synaptic depression at a fast central synapse. *Neuron.* 20:797–807.

Haack, J. A., and R. L. Rosenberg. 1994. Calcium-dependent inactivation of L-type calcium channels in planar lipid bilayers. *Biophys. J.* 66: 1051–1060.

Hadley, R. W., and W. J. Lederer. 1991. Ca^{2+} and voltage inactivate Ca^{2+} channels in guinea-pig ventricular myocytes through independent mechanisms. *J. Physiol. (Lond.).* 444:257–268.

Herlitze, S., G. H. Hockerman, T. Scheuer, and W. A. Catterall. 1997. Molecular determinants of inactivation and G protein modulation in the intracellular loop connecting domains I and II of the calcium channel α_{1A} subunit. *Proc. Natl. Acad. Sci. USA.* 94:1512–1516.

Ho, S. N., H. D. Hunt, R. M. Horton, J. K. Pullen, and L. R. Pease. 1989. Site-directed mutagenesis by overlap extension using the polymerase chain reaction. *Gene.* 77:51–59.

Hoshi, T., W. N. Zagotta, and R. W. Aldrich. 1990. Biophysical and molecular mechanisms of *Shaker* potassium channel inactivation. *Science.* 250:533–538.

Imredy, J. P., and D. T. Yue. 1992. Submicroscopic Ca^{2+} diffusion mediates inhibitory coupling between individual Ca^{2+} channels. *Neuron.* 9:197–207.

Imredy, J. P., and D. T. Yue. 1994. Mechanism of Ca^{2+}-sensitive inactivation of L-type Ca^{2+} channels. *Neuron.* 12:1301–1318.

Johnson, B. D., and L. Byerly. 1993. A cytoskeletal mechanism for Ca^{2+} channel metabolic dependence and inactivation by intracellular Ca^{2+}. *Neuron.* 10:797–804.

Kass, R. S., and M. C. Sanguinetti. 1984. Inactivation of calcium channel current in the calf cardiac Purkinje fiber. Evidence for voltage- and calcium-mediated mechanisms. *J. Gen. Physiol.* 84:705–726.

Kiss, L., and S. J. Korn. 1998. Modulation of C-type inactivation by K^+ at the potassium selectivity filter. *Biophys. J.* 74:1840–1849.

Klockner, U., G. Mikala, M. Varadi, G. Varadi, and A. Schwartz. 1995. Involvement of the carboxyl-terminal region of the alpha 1 subunit in voltage-dependent inactivation of cardiac calcium channels. *J. Biol. Chem.* 270:17306–17310.

Kohama, K. 1979. Divalent cation binding properties of slow skeletal muscle troponin in comparison with those of cardiac and fast skeletal muscle troponins. *J. Biochem.* 86:811–820.

Kramer, R. H., L. K. Kaczmarek, and E. S. Levitan. 1991. Neuropeptide inhibition of voltage-gated calcium channels mediated by mobilization of intracellular calcium. *Neuron.* 6:557–563.

Kretsinger, R. H. 1976. Calcium-binding proteins. *Annu. Rev. Biochem.* 45:239–266.

Lee, K. S., E. Marban, and R. W. Tsien. 1985. Inactivation of calcium channels in mammalian heart cells: joint dependence on membrane potential and intracellular calcium. *J. Physiol. (Lond.).* 334:395–411.

Liu, Y., M. E. Jurman, and G. Yellen. 1996. Dynamic rearrangement of the outer mouth of a K^+ channel during gating. *Neuron.* 16:859–867.

Lòpez-Barneo, J., T. Hoshi, S. H. Heinemann, and R. W. Aldrich. 1993. Effects of external cations and mutations in the pore region on C-type inactivation of *Shaker* potassium channels. *Receptors Channels.* 1:61–71.

Lòpez-Lòpez, J. R., P. S. Shacklock, C. W. Balke, and W. G. Wier. 1995. Local calcium transients triggered by single L-type calcium channel currents in cardiac cells. *Science.* 268:1042–1045.

Mejia-Alvarez, R., M. Fill, and E. Stefani. 1991. Voltage-dependent inactivation of t-tubular skeletal muscle calcium channels in planar lipid bilayers. *J. Gen. Physiol.* 97:393–412.

Neely, A., R. Olcese, X. Wei, L. Birnmbaumer, and E. Stefani. 1994. Ca^{2+}-dependent inactivation of a cloned cardiac Ca^{2+} channel α_1 subunit (α_{1C}) expressed in *Xenopus* oocytes. *Biophys. J.* 66:1895–1903.

Noceti, F., R. Olcese, N. Qin, J. Zhou, and E. Stefani. 1998. Effect of Bay K8644 (−) and the β_{2a} subunit on Ca^{2+}-dependent inactivation in α_{1C} Ca^{2+} channels. *J. Gen. Physiol.* 111:463–475.

Obejero-Paz, C. A., S. W. Jones, and A. Scarpa. 1991. Calcium currents in the A7r5 smooth muscle-derived cell line: increase in current and selective removal of voltage-dependent inactivation by intracellular trypsin. *J. Gen. Physiol.* 98:1127–1140.

Parent, L., and M. Gopalakrishnan. 1995. Glutamate substitution in repeat IV alters monovalent and divalent permeation in the heart α_{1C} calcium channel. *Biophys. J.* 69:1801–1813.

Parent, L., M. Gopalakrishnan, A. E. Lacerda, X. Wei, and E. Perez-Reyes. 1995. Voltage-dependent inactivation in cardiac-skeletal chimeric calcium channels. *FEBS Lett.* 360:144–150.

Parent, L., T. Schneider, C. Porter Moore, and D. Talwar. 1997. Subunit regulation of the human brain α_{1E} calcium channel. *J. Membr. Biol.* 160:127–139.

Patil, P. G., D. L. Brody, and D. T. Yue. 1998. Preferential closed-state inactivation of neuronal calcium channels. *Neuron.* 20:1027–1038.

Perez-Reyes, E., A. Castellano, H. S. Kim, P. Bertrand, E. Baggstrom, A. E. Lacerda, X. Wei, and L. Birnbaumer. 1992. Cloning and expression of a cardiac/brain β subunit of the L-type calcium channel. *J. Biol. Chem.* 267:1792–1797.

Perez-Reyes, E., L. Cribbs, A. Daud, A. E. Lacerda, J. Barclay, M. P. Williamson, M. Fox, M. Rees, and J. H. Lee. 1998. Molecular characterization of a neuronal low-voltage-activated T-type calcium channel. *Nature.* 391:896–900.

Perez-Reyes, E., X. Wei, A. Castellano, and L. Birnbaumer. 1990. Molecular diversity of L-type calcium channels. Evidence for alternative splicing of the transcripts of three non-allelic genes. *J. Biol. Chem.* 265:20430–20436.

Porter Moore, C., D. Talwar, and L. Parent. 1997. Role of glutamate residue E1537 in calcium-dependent inactivation of α_{1C} calcium channels. *Biophys. J.* 72:A146 (Abstr.).

Risso, S., and L. J. DeFelice. 1993. Ca channel kinetics during the spontaneous heart beat in embryonic chick ventricle cells. *Biophys. J.* 65: 1006–1018.

Sambrook, J., E. F. Fritsch, and T. Maniatis. 1989. Molecular Cloning: A Laboratory Manual. Cold Spring Harbor Laboratory, Cold Spring Harbor, NY.

Soldatov, N. M., R. D. Zühlke, A. Bouron, and H. Reuter. 1997. Molecular structures involved in L-type calcium channel inactivation. *J. Biol. Chem.* 272:3560–3566.

Tsien, R. W. 1998. Key clockwork component cloned. *Nature.* 391:839–841.

Wei, X., E. Perez-Reyes, A. E. Lacerda, G. Schuster, A. M. Brown, L. Birnbaumer. 1991. Heterologous regulation of the cardiac Ca^{2+} channel α_1 subunit by skeletal muscle β and "gamma" subunits. Implications for the structure of the cardiac L-type Ca^{2+} channels. *J. Biol. Chem.* 266:21943–21947.

West, J. M., D. E. Patton, T. Scheuer, Y. Wang, A. L.. Goldin, and W. A. Catterall. 1992. A cluster of hydrophobic amino acid residues required for fast Na^+-channel inactivation. *Proc. Natl. Acad. Sci. USA.* 89: 10910–10914.

White, M. M., and M. Aylwin. 1990. Niflumic and flufenamic acids are potent reversible blockers of Ca^{2+}-activated Cl^- channels in *Xenopus* oocytes. *Mol. Pharmacol.* 37:227–229.

Williams, M. E., D. H. Feldman, A. F. McCue, R. Brenner, G. Velicelebi, S. B. Ellis, and M. M. Harpold. 1992. Structure and functional expression of α_1, α_2, and β subunits of a novel human neuronal calcium channel subtype. *Neuron.* 8:71–84.

You, Y., D. J. Pelzer, and S. Pelzer. 1995. Trypsin and forskolin decrease the sensitivity of L-type calcium current to inhibition by cytoplasmic free calcium in guinea pig heart muscle cells. *Biophys. J.* 69:1838–1846.

Zhang, J. F., P. T. Ellinor, R. W. Aldrich, and R. W. Tsien. 1994. Molecular determinants of voltage dependent inactivation in calcium channels. *Nature.* 372:97–100.

Zhou, J., R. Olcese, N. Qin, F. Noceti, L. Birnbaumer, and E. Stefani. 1997. Feedback inhibition of Ca^{2+} channels by Ca^{2+} depends on a short sequence of the C-terminus that does not include the Ca^{2+}-binding function of a motif with similarity to Ca^{2+}-binding domains. *Proc. Natl. Acad. Sci. USA.* 94:2301–2305.

Zühlke, R. D., and H. Reuter. 1998. Ca^{2+}-sensitive inactivation of L-type Ca^{2+} channels depends on multiple cytoplasmic amino acid sequences of the α_{1C} subunit. *Proc. Natl. Acad. Sci. USA.* 95:3287–3294.